Fachtagung "Lasermethoden in der Strömungsmesstechnik"
6. – 8. September 2016, Cottbus

Taylor-Couette Turbulenz in weiten und sehr weiten Spalten

Taylor-Couette turbulenz at wide and very wide gaps

Andreas Froitzheim[1], Sebastian Merbold[1], Christoph Egbers[1]
[1] Lehrstuhl Aerodynamik und Strömungslehre, Brandenburgisch Technische Universität Cottbus-Senftenberg, Siemens-Halske-Ring 14, 03046-Cottbus, Germany

Schlagworte: PIV-Couette, Turbulenz, Drehmoment, PIV, weite und sehr weite Spalte
Keywords: Taylor-Couette, turbulence, angular momentum, PIV, wide and very wide gaps

Summary

The angular momentum transport in a Taylor-Couette flow features a dominant maximum in the low counter rotating regime. We analyzed with PIV the fully turbulent flow field in a wide gap experiment in this regime finding dominant Taylor vortices. Due to reconstruction of the axial velocity component we also quantified the strength of these vortices, which increases with increasing shear Reynolds number.

Introduction

A classical experiment to investigate the physics of rotating fluids is the Taylor-Couette (TC) system. Therein, the flow is surrounded by two concentric cylinders, which can rotate independently in co- or counter direction. With the radii of the inner r_1 and outer cylinder r_2 and the length of these cylinders L, the geometry is defined by the radius ratio $\eta=r_1/r_2$, the gap width $d=r_2-r_1$ and the aspect ratio $\Gamma=L/d$. The angular velocities of both cylinders $\omega_{1,2}$ are used to describe the kinematic similarity by the shear Reynolds number Re_S (see Dubrulle et al. 2005) and the dynamic similarity by the rotation ratio $\mu=\omega_2/\omega_1$:

$$Re_S = \frac{2r_1r_2d}{\nu(r_1+r_2)}|\omega_2-\omega_1| \qquad (1)$$

Our experimental study is focused on the angular momentum transport J^ω and the underlying flow structure in wide gap and very wide gap fully turbulent Taylor-Couette flows, where curvature effects come into account. Concerning this matter special attention is paid to the dependence of J^ω on the rotation ratio μ at constant Re_S. Here, a maximum in the transport occurs in the low counter rotating regime ($\mu_{max}(\eta=0.5)=-0.2$) due to an increase of the remnants of the turbulent Taylor vortices (see Brauckmann & Eckhardt 2013, Merbold et al. 2013, Merbold et al. 2014, Ostilla-Mónico et al. 2014a,b). Therefore we measure the torque, which is directly connected to the angular momentum transport according to Eckhardt et al. (2007). Further we perform PIV measurements in the radial-azimuthal plane at different axial positions to quantify the velocity field and therefore the turbulent Taylor vortices (see also Van der Veen at al. 2015).

Experimental Setup

The Taylor-Couette apparatus used for the experiments presented here is pictured in Fig. 1. The inner cylinder is mounted on an inner shaft, which allows us to build in different inner

Karlsruhe, Germany, ISBN 978-3-9816764-2-6

cylinders with the radii r_1=7mm, 25mm and 35mm. The outer cylinder (r_2=70mm) and the top plate are made of acrylic glass to enable optical access. The end plates are fixed to the outer cylinder and enclose the gap at a length of L=700mm. So we can realize gap widths of d=63mm, 45mm and 33mm, radius ratios of η=0.1, 0.357 and 0.5 and aspect ratios of Γ=11.1, 15.6 and 20 respectively. In the case of η=0.5 we can reach shear Reynolds numbers up to $Re_S=3\cdot10^5$. Within this paper we investigated a wide gap Taylor-Couette flow with η=0.5, Γ=20 and distilled water as working fluid with a kinematic viscosity of $\nu=10^{-6}$.

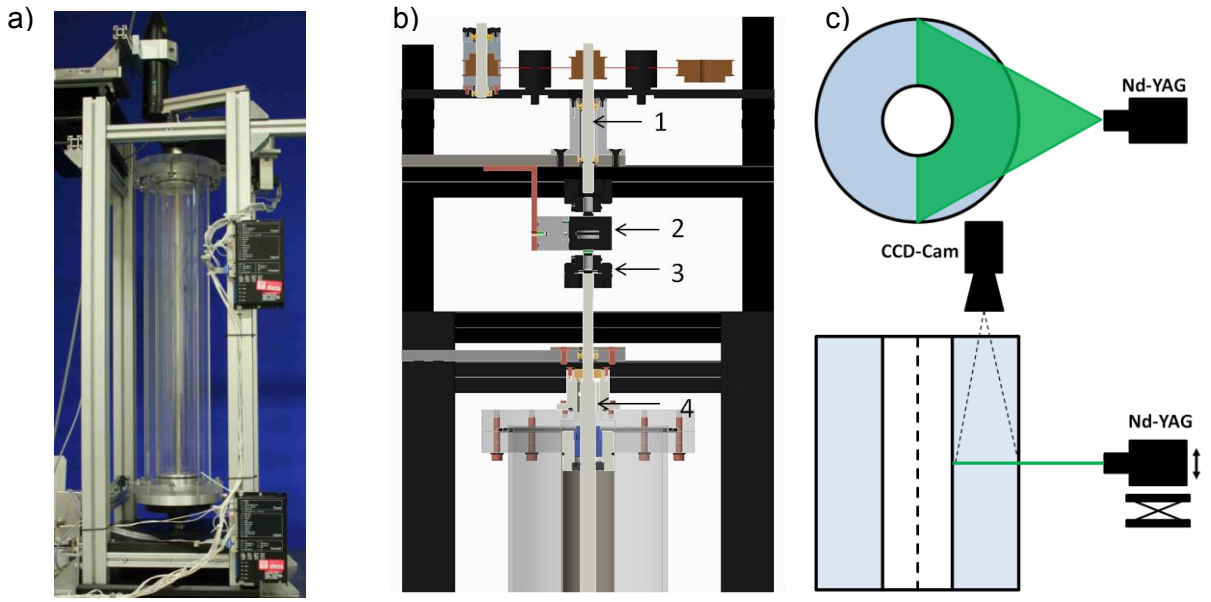

Fig. 1 a) Photograph of the Taylor-Couette facility; b) Drawing of the torque measurement system with driving shaft (1), shaft to shaft rotary torque sensor (2), torsionally stiff coupling (3) and inner TC shaft (4); c) sketch of the PIV set up.

The torque is measured in our system using a shaft to shaft rotary torque sensor (±1Nm, 0.1% precision) in the driving chain mounted with torsionally stiff couplings between the motor of the inner cylinder and the inner shaft. Consequently our torque signal includes end wall effects and friction forces of the bearings. The latter one can be subtracted by measuring the acting torque with air, as this signal will be dominated by the friction forces.

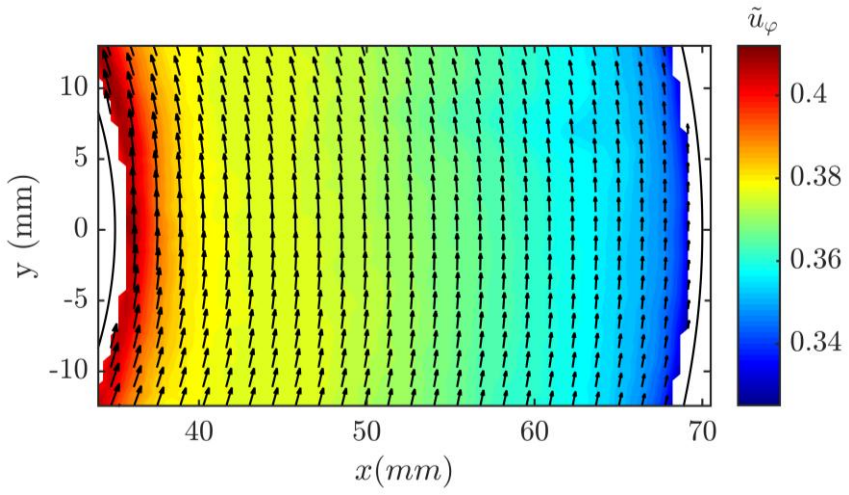

Fig. 2: Temporal and spatial averaged, normalized azimuthal velocity component in a horizontal plane at η=0.5, $Re_S=8\cdot10^4$ and μ=-0.2.

To analyze the flow structure PIV measurements are performed in the radial-azimuthal plane at different axial positions H (see Fig. 2). Beside the experiment a Nd-YAG laser (λ=532 nm) is mounted on a traverse creating a 2 mm thick light sheet in the axial range of 0.571<H/L<0.686 with 4 mm resolution, leading to 21 axial positions. The distilled water is seeded with hollow glass spheres scattering the laser light, which is captured by a CCD camera (1600x1200 px) mounted on top of the experiment above the transparent top plate. The spatial resolution is in the interval of Δ(x,y)=[0.379 mm, 0.46 mm] depending on the axial position within a segment of circle of φ=[20.92°, 25.46°] related to the outer cylinder. With this setup the radial u_r and azimuthal u_φ velocity components are measured. Each measurement consists of 150 double images recorded with 15 Hz.

Angular momentum transport and underlying flow structure

The comparative investigation of direct torque and PIV measurements in a wide gap TC flow will be done by varying the rotation ratio μ at a constant shear Reynolds number Re_S. In Fig. 3 the Nusselt number and the time and spatial (φ) averaged normalized radial velocity component are shown for different μ at $Re_S=[8;8.4]\cdot10^4$. The normalized radial coordinate ř and radial velocity component $\tilde{u}_r$ are defined as $\check{r}=(r-r_1)/(r_2-r_1)$ and $\tilde{u}_r=u_r/u_s$ with the shear velocity $u_s=(Re_S\ \nu)/d$. The angular momentum transport increases with decreasing μ from an outer cylinder at rest (μ=0) to a maximum in the low counter rotating regime (μ_{max}=-0.2). For higher counter rotating rates Nu_ω decreases again. A better understanding of this behavior is given by the contour plot of the radial velocity component in terms of the axial and radial coordinate, created out of 21 single PIV measurements at different axial positions.

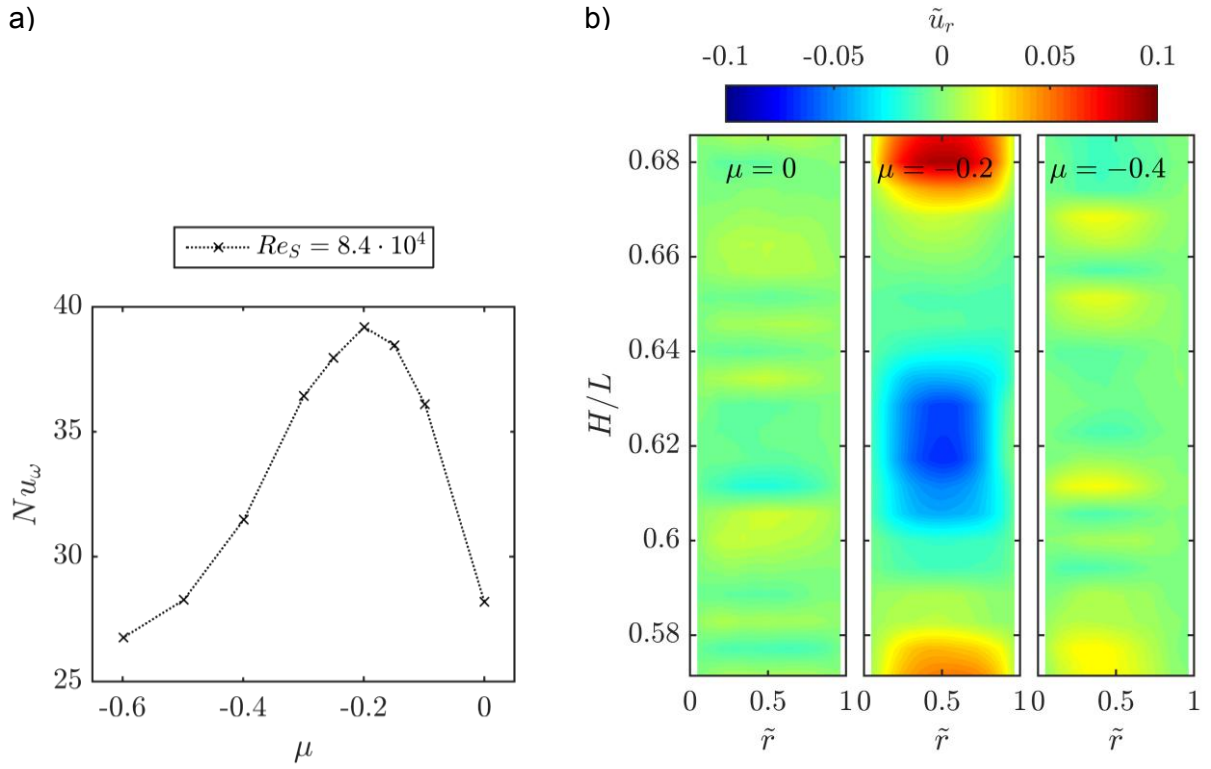

Fig. 3: a) Angular momentum transport as function of the rotation ratio μ for $Re_S=8.4\cdot10^4$; b) Contour plots of the temporal and azimuthally averaged, normalized radial velocity component $\tilde{u}_r$ at 21 different axial positions H for $Re_S=8\cdot10^4$.

For μ=0 the radial velocity is nearly zero in the flow. The alternating regions of small positive and negative radial velocity are assumed to be remnants of turbulent Taylor vortices. At the torque maximum strong roll structures evolve in the flow and fill the whole gap. These vorti-

ces seem to cause the maximum in the angular momentum transport. When the rotation ratio is further decreased to μ=-0.4 the dominant roll structures are not detectable any more. However, similar to the case of an outer cylinder at rest, alternating regions of positive and negative radial velocity appear. The intensity is higher than for μ=0, but these regions are restricted to an inner part of the gap. This flow behavior indicates the stabilizing of the flow by the outer cylinder rotation leading to a decrease of the torque. The most important result however is that also in a fully turbulent Taylor-Couette flow turbulent Taylor vortices can arise in the gap as dominant pattern. In the following we want to investigate these vortices in more detail.

Reconstruction of the axial velocity component u_z at $\mu=\mu_{max}$

Taylor vortices lead to an ordered secondary flow in the gap causing an increased radial and axial velocity component. Therefore the axial velocity component in addition to the radial one is crucial to examine these vortices. As we performed PIV measurements in the radial-azimuthal plane at different heights, the axial velocity component can be reconstructed. Hereby it is important to note that the measurements at the different cylinder heights have been done at different times. Accordingly this reconstruction is only possible for the time and azimuthal averaged flow field containing stationary vortices. As can be seen in Fig. 3b this condition is fulfilled. The reconstruction is based on the time averaged, incompressible continuity equation in cylindrical coordinates:

$$\frac{\partial u_z}{\partial z} = -\frac{\partial u_r}{\partial r} - \frac{u_r}{r} - \frac{1}{r}\frac{\partial u_\varphi}{\partial \varphi} \qquad (2)$$

The partial derivatives of the radial and azimuthal velocity components are calculated using a central differential scheme at each axial height for the time averaged PIV data. In a next step these derivatives are averaged over the azimuthal coordinate. Now, using equation 2 the axial gradient of u_z can be calculated in a vertical sheet. To evaluate subsequently the axial velocity component, u_z has to be known at least at one axial position for all radial locations. As the measurement volume is in the middle section of the cylinder no boundary conditions of the top or bottom plate are accessible. Therefore the axial profile of the radial velocity component is used. At the in- and outflow regions of a Taylor vortex, the axial velocity component vanishes and the radial velocity component has its extreme values. Thus we determine the axial location of the minimum of the radial velocity component using a harmonic fit at all radial position (see Fig. 4).

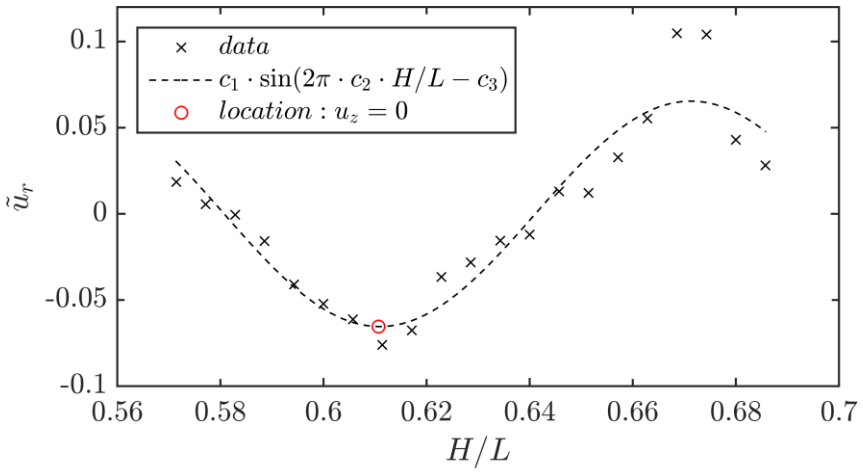

Fig. 4: Normalized radial velocity profile along the axial direction at mid gap (ř=0.5) for $Re_S=10^5$ and μ=-0.2 (crosses). The dashed line represents a harmonic fit. The red circle represents the minimum of the profile, where the axial velocity component vanishes.

The uncertainty of this fit numbered by the root mean square error is taken into account by changing this zero position of the axial velocity in the error interval. The location of vanishing u_z is chosen for the spatial averaged minimum difference in the kinetic energy of the radial and axial velocity component. A second order interpolation scheme is used for the evaluation of the gradients. The result of the velocity field in the vertical plane is pictured in Fig. 5 for different shear Reynolds numbers. The crosses in Fig. 5 represent the centers of the vortices. The position is estimated by the location of the minimum of the kinetic wind energy $\min(e_{kin,w})=\min(0.5\cdot u_z^2+0.5\cdot u_r^2)$. For all investigated shear Reynolds numbers the vortex centers are located more close to the outer than to the inner cylinder wall leading to a weak acceleration of the wind in the outer gap region. Further the vortices are slightly tilted, while the in- and outflow regions seem to be horizontal in its center. However the width of the inflows increases and the width of the outflows decreases in positive radial direction.

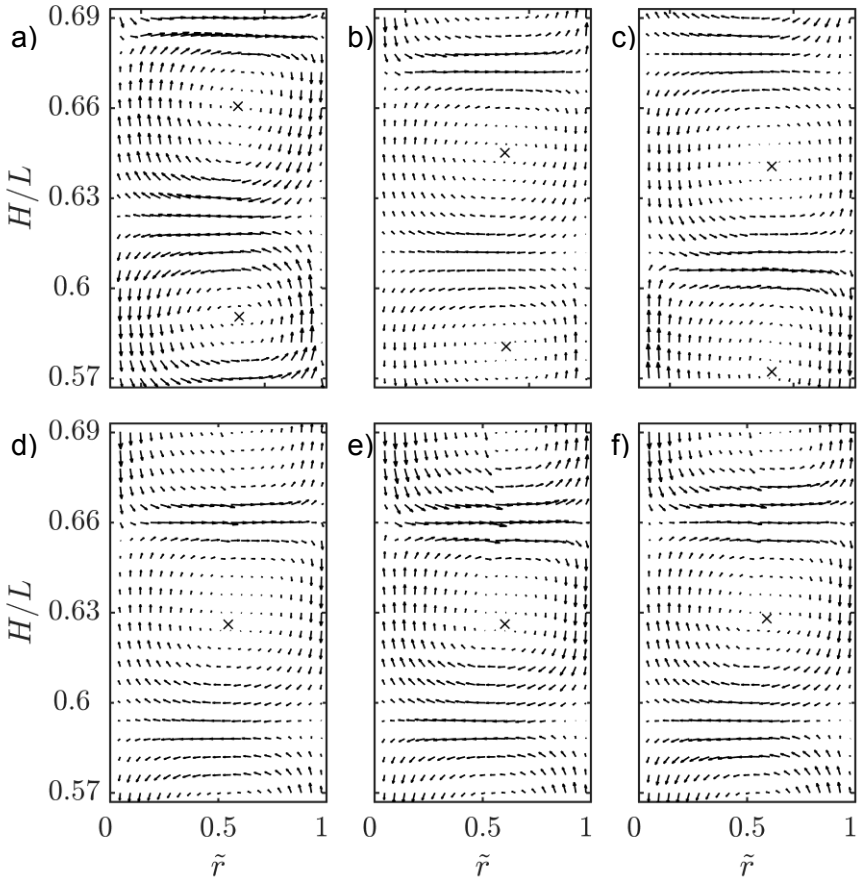

Fig. 5: Reconstructed vector plots of the temporal and spatial averaged radial-axial velocity field for different shear Reynolds numbers: a) $Re_S=8\cdot10^4$, b) $Re_S=1\cdot10^5$, c) $Re_S=1.65\cdot10^5$, d) $Re_S=1.92\cdot10^5$, e) $Re_S=2.01\cdot10^5$, f) $Re_S=2.19\cdot10^5$. The black crosses indicate the locations of the vortex centers.

Strength of Taylor vortices

The two dimensional flow field in the axial-radial plane enables a quantitative comparison of the vortex strength for different shear Reynolds numbers. An appropriate parameter is the circulation Γ:

$$\Gamma = \oint u_i dx_i \tag{3}$$

We can evaluate the line integral along concentric circles around the vortex center with different radii $\check{r}_\Gamma = r_\Gamma/d$ at 0.001 mm ≤ r_Γ ≤ 0.013 mm. The restriction to this radius range is due to the shifted location of the vortex centers from the centerline. Fig. 6a shows the circulation as a function of $\check{r}_\Gamma$ for different Re_S:

Karlsruhe, Germany, ISBN 978-3-9816764-2-6

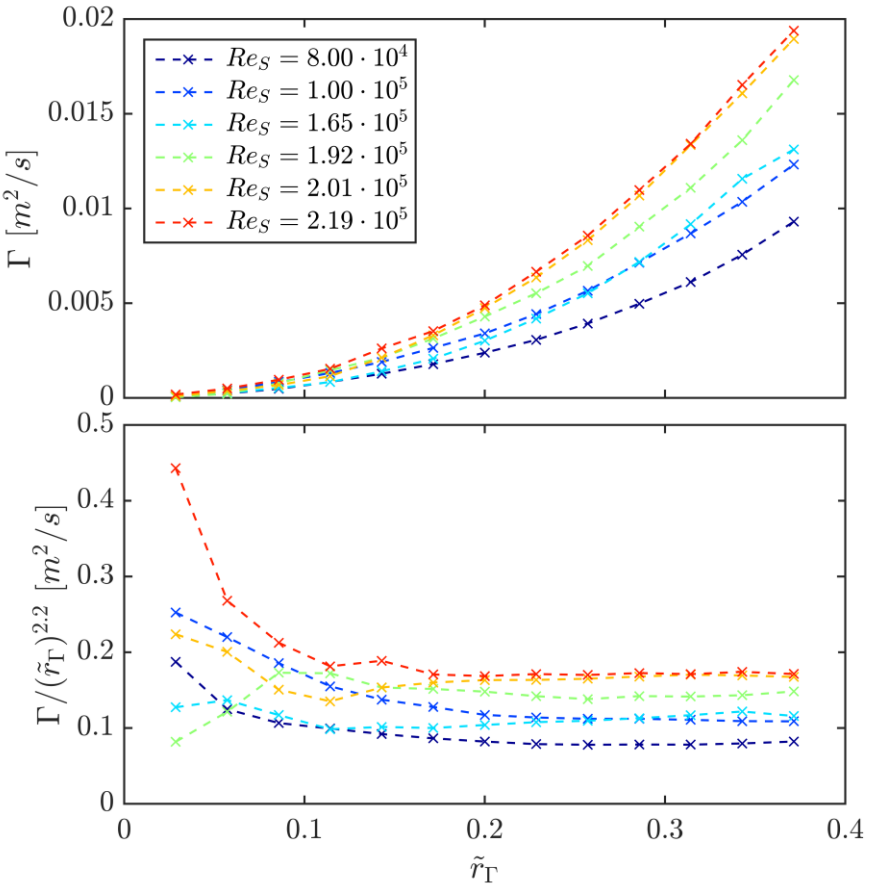

Fig. 6: a) Circulation Γ as function of the evaluating radius $\check{r}_\Gamma$ for different Re_S; b) Compensated circulation as function of the evaluating radius $\check{r}_\Gamma$ for different Re_S.

The circulation of the vortices increases with the chosen radius exponentially for all shear Reynolds numbers. Further for large enough $\check{r}_\Gamma$, Γ also increases with Re_S leading to the question of the right choice of $\check{r}_\Gamma$. Assuming the relation $\Gamma \sim \check{r}_\Gamma^{\gamma}$ to hold we performed a power law fit resulting in γ=2.2 for all Re_S. In Fig. 6b the compensated circulation is pictured using this scaling relation. For small radii $\check{r}_\Gamma$ the circulation strongly changes with increasing $\check{r}_\Gamma$. However when $\check{r}_\Gamma$=0.25 is reached, the circulation stays constant. Consequently we choose the highest possible radius $\check{r}_\Gamma$=0.37 for analyzing the dependence of the circulation from the shear Reynolds number to ensure that the influence of the evaluating radius of Γ is negligible. In Fig. 7 the compensated circulation is pictured at $\check{r}_\Gamma$=0.37. The circulation of the Taylor vortices increases slightly with increasing shear Reynolds number. The low growth rate is illustrated by a linear curve with a slope of $5.7 \cdot 10^{-7}$. In Taylor-Couette flows a still open question is whether or not turbulent Taylor vortices can survive for arbitrarily high Reynolds numbers. As can be seen from Fig. 3b, the vortices disappear inside the gap for pure inner cylinder rotation. Further at the torque maximum region they appear again. From our circulation analysis the increasing trend of the vortex strength suggests that the Taylor vortices will survive for all shear Reynolds numbers.

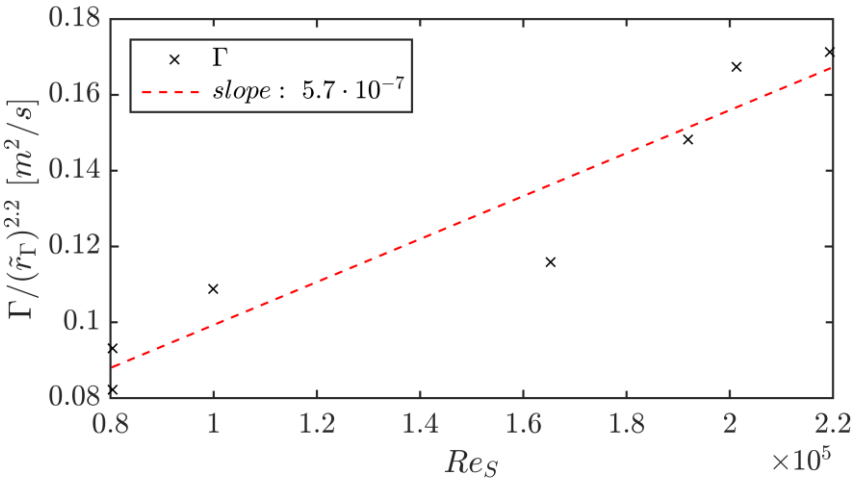

Fig. 7: Compensated circulation Γ as function of the shear Reynolds number (crosses). Dashed line represents a linear curve with slope $5.7 \cdot 10^{-7}$ to guide the eye.

Concluding we analyzed the flow structure in the vicinity of the maximal angular momentum transport finding dominant Taylor vortices inside the gap. Further we could quantify the strength of these vortices by reconstructing the axial velocity component showing an increase with the shear Reynolds number. As 2D2C PIV measurement in a vertical plane are restricted to low shear Reynolds numbers due to the dominant out of plane velocity, horizontal PIV measurements at different axial locations are applicable to at least investigate the mean 3D flow.

Acknowledgements

We gratefully acknowledge financial support by the Deutsche Forschungsgemeinschaft (DFG FOR 1182, EG 100/ 15-1, EG 100/ 15-2).

References

Brauckmann H. J. and Eckhardt B., (2013): Intermittent boundary layers and torque maxima in Taylor-Couette flow, Phys. Rev. E87, 033004

Dubrulle, B., Dauchot, F., Longaretti, P.Y., Richard, D., Zahn, J.P., 2005: “Stability and turbulent transport in Taylor-Couette flow from analysis of experimental data”, Phys. Fluids 17, 095103.

Eckhardt, B., Grossman, S., Lohse, D., 2007: “Torque scaling in turbulent Taylor-Couette flow between independently rotating cylinders”, Journal of Fluid Mechanics, Vol. 581, pp. 221-250

Merbold, S., Froitzheim, A., Egbers, C., 2014: “Flow pattern and angular motion transport in a wide gap Taylor-Couette flow”, TU Dresden, Strömungstechnische Tagung 2014, Schriftenreihe aus dem Institut für Strömungsmechanik Band 10

Merbold, S., Brauckmann, H.J., Egbers, C., 2013: „Torque measurements and numerical determination in differentially rotating wide gap Taylor-Couette flow”, Phys. Rev. E87, 023014

Ostilla-Mónico, R., van der Poel, E.P., Verzicco, R., Grossmann, S., Lohse, D., 2014a: „Exploring the phase diagram of fully turbulent Taylor-Couette flow”, Journal of Fluid Mechanics, Vol. 761, pp. 1-26

Ostilla-Mónico, R., Huisman, S.G., Jannink, T.J.G., van Gils, D.P.M., Verzicco, R., Grossmann, S., Sun, C., Lohse, D., 2014b: “Optimal Taylor-Couette flow: radius ratio dependence”, Journal of Fluid Mechanics, Vol. 747, pp. 1-29

Van der Veen, R. C. A., Huisman, S. G., Merbold, S., Harlander, U., Egbers, C., Lohse, D. & Sun, C., 2016: "Taylor-Couette turbulence at radius ratio η=0.5: scaling, flow structures and plumes", arXiv:1508.05802.

Karlsruhe, Germany, ISBN 978-3-9816764-2-6